

## Selectively-Sized Graphene-Based Nanopores for In-situ Single Molecule Sensing

Colin Roger Crick, Jasmine Y. Y. Sze, Martin Rosillo-lopez, Christoph G Salzmann, and Joshua B. Edel

*ACS Appl. Mater. Interfaces*, **Just Accepted Manuscript** • Publication Date (Web): 24 Jul 2015

Downloaded from <http://pubs.acs.org> on July 24, 2015

### Just Accepted

“Just Accepted” manuscripts have been peer-reviewed and accepted for publication. They are posted online prior to technical editing, formatting for publication and author proofing. The American Chemical Society provides “Just Accepted” as a free service to the research community to expedite the dissemination of scientific material as soon as possible after acceptance. “Just Accepted” manuscripts appear in full in PDF format accompanied by an HTML abstract. “Just Accepted” manuscripts have been fully peer reviewed, but should not be considered the official version of record. They are accessible to all readers and citable by the Digital Object Identifier (DOI®). “Just Accepted” is an optional service offered to authors. Therefore, the “Just Accepted” Web site may not include all articles that will be published in the journal. After a manuscript is technically edited and formatted, it will be removed from the “Just Accepted” Web site and published as an ASAP article. Note that technical editing may introduce minor changes to the manuscript text and/or graphics which could affect content, and all legal disclaimers and ethical guidelines that apply to the journal pertain. ACS cannot be held responsible for errors or consequences arising from the use of information contained in these “Just Accepted” manuscripts.



# Selectively-Sized Graphene-Based Nanopores for In-situ Single Molecule Sensing

*Colin R. Crick<sup>†#</sup>, Jasmine Y. Y. Sze<sup>†#</sup>, Martin Rosillo-Lopez<sup>‡</sup>, Christoph G. Salzmann<sup>‡</sup> and  
Joshua B. Edel<sup>†\*</sup>*

<sup>†</sup> Department of Chemistry, Imperial College London, South Kensington Campus, London, SW7  
2AZ, United Kingdom

<sup>‡</sup> Department of Chemistry, University College London, 20 Gordon Street, London, WC1H 0AJ,  
United Kingdom

<sup>#</sup> These authors contributed equally to the manuscript

KEYWORDS – Nanopore, Graphene, DNA, Translocation, Graphene Nanoflake, Size Tuning.

ABSTRACT - The use of nanopore biosensors is set to be extremely important in developing precise single molecule detectors, and providing highly sensitive advanced analysis of biological molecules. The precise tailoring of nanopore size is a significant step toward achieving this, as it would allow for a nanopore to be tuned to a corresponding analyte. The work presented within

1  
2  
3 details a methodology for selectively opening nanopores in real-time. The tuneable nanopores on  
4 a quartz nanopipette platform are fabricated using the electroetching of a graphene-based  
5 membrane constructed from individual graphene nanoflakes ( $\varnothing = 30$  nm). The device design  
6 allows for in-situ opening of the graphene membrane, from fully closed to fully opened ( $\varnothing = 25$   
7 nm), a feature that has yet to be reported in the literature. The translocation of DNA is studied as  
8 the pore size is varied, allowing for sub-features of DNA to be detected with slower DNA  
9 translocations at smaller pore sizes, and the ability to observe trends as the pore is opened. This  
10 approach opens the door to creating a device that can be target to detect specific analytes.  
11  
12  
13  
14  
15  
16  
17  
18  
19  
20  
21  
22

## 23 **Introduction**

24  
25  
26  
27 The development of comprehensive and efficient analysis techniques for biological molecules  
28 is a rapidly growing area of research.<sup>1-4</sup> A range of methods have recently been reported for the  
29 advanced analysis of single biological molecules.<sup>5-8</sup> Plausible outcomes in the future  
30 development of devices in this class would be to probe protein-nanopore interactions, protein-  
31 protein interactions, and eventually the ability to read the base pairs of DNA molecules by  
32 achieving higher special resolution, and requiring only a single molecule to do so.<sup>9,10</sup> One  
33 category of these devices are nanopores, which are nanometre-sized holes which have been used  
34 in devices aimed towards detecting a range of molecules, including DNA and proteins.<sup>11-14</sup> The  
35 general principles of detection are grounded in passing biological molecules through a nanopore  
36 (translocation) by application of an electric field, and observing experimental responses, such as  
37 the ionic current. Further detection strategies also exist including use of tunnelling currents,  
38 fluorescence, and surface-enhanced Raman spectroscopy, which can be carried out  
39 independently or employed as a synchronised detection platform.<sup>15-17</sup>  
40  
41  
42  
43  
44  
45  
46  
47  
48  
49  
50  
51  
52  
53  
54  
55  
56  
57  
58  
59  
60

1  
2  
3 Major milestones for nanopore single molecule detection are the effective analysis of  
4 molecular components.<sup>18,19</sup> There are many well-established nanopore systems in the scientific  
5 literature are capable of approximating molecular charge, size and conformations.<sup>20-22</sup> The  
6 determination of further molecular properties has been reported, including the identification of  
7 molecular branching, in addition to probing the variations of molecular interaction with the  
8 nanopore surfaces.<sup>18,23-25</sup> These systems are dependent on the precise tailoring of nanopore size  
9 (diameter and length), in addition to the material it is constructed from. The diameter of the  
10 nanopore must be large enough to allow the molecular analyte to fit through, however a very  
11 large pore would result in an insignificant signal, making analysis increasingly difficult.<sup>26</sup> The  
12 material of the nanopore device also hugely influences the nature of interaction with the  
13 molecule as the translocation occurs, as an attraction or repulsion force may be present. This has  
14 been shown in many studies which examine nanopore surface functionalisation.<sup>27</sup> The general  
15 principle of this approach is to cause an interaction to occur as the molecule translocates through  
16 the pore. This can be in an attractive force (including hydrogen bonds and Van Der Waals  
17 interactions) used to slow down the translocation speed, or a repulsive force (including large  
18 columbic forces), which may act to shrink the appreciable pore diameter.  
19  
20  
21  
22  
23  
24  
25  
26  
27  
28  
29  
30  
31  
32  
33  
34  
35  
36  
37  
38  
39  
40

41  
42 The precise configuration of successful nanopore devices varies with respect to the specific  
43 analyte under investigation, in addition to the environmental conditions of the experiment (i.e.  
44 solution concentrations, applied potentials, etc...).<sup>28,29</sup> A result of this is an aspiration for devices  
45 to be tuneable, so that a range of molecules can be used without the need for designing,  
46 fabricating and testing a new device architecture. Electron beams, plasma etching, material  
47 deposition and surface functionalisation have been used to control the shapes and size of  
48 nanopores.<sup>30-33</sup> Materials including graphene have been utilised due to their high mechanical  
49  
50  
51  
52  
53  
54  
55  
56  
57  
58  
59  
60

1  
2  
3  
4 strength, this enables free standing membranes to be formed to support a nanopore, in addition to  
5  
6 widely reported low electrical noise and selectivity.<sup>34-40</sup> The graphene membranes used in the  
7  
8 construction of these devices is exclusively single/multi-layer graphene sheets suspended over  
9  
10 voids. These sheets are then targeted for nanopore milling, primarily using electron and ion  
11  
12 beams.  
13  
14

15  
16 Previous literature reports the ability to select the size of nanopores supported on graphene  
17  
18 membranes, however the size of the pore must be determined before any bio-sensing  
19  
20 experiment.<sup>8,26,41-43</sup> Electrochemical opening alongside DNA translocation experiments have  
21  
22 been reported on molybdenum sulphide and silicon nitride free-standing membranes.<sup>44-46</sup> Recent  
23  
24 reports have covered both the electrochemistry and the electrochemical etching of graphene  
25  
26 membranes however, the techniques involve a substantial amount of fabrication.<sup>47,48</sup> Relying  
27  
28 upon cleanroom fabrication of nanopore devices and single layered graphene.  
29  
30  
31

32  
33 The work presented in this article aims to use multi-layered graphene films to completely  
34  
35 cover our nanopipette (see supplementary information for full experimental details). The aim of  
36  
37 the experiments was to completely coat the pore at the end of the nanopipettes using water  
38  
39 dispersed graphene nanoflakes (GNFs). The GNFs used in the experiment are small portions of  
40  
41 single layered graphene ( $\varnothing \sim 30$  nm) that are able to be dispersed in a solvent (Figure 1C).<sup>49</sup>  
42  
43 Graphitic films are formed by annealing the GNF coated nanopipettes in a vacuum oven. The  
44  
45 nanopore coating is analysed using ionic conductivity measurements. Alternating current (AC) is  
46  
47 used to etch away the membrane material, with the frequency, applied potential and overall  
48  
49 treatment length tuned for steady pore opening. The AC opening technique provides the  
50  
51 opportunity for graphene membrane etching, electrical testing and DNA translocations to be  
52  
53 performed without interruption. The translocation of DNA is carried out as the pores are opened,  
54  
55  
56  
57  
58  
59  
60

1  
2  
3 any observed difference in DNA behaviour is related to the effect of nanopore size. The reported  
4  
5 technique aims to demonstrate precise, in-situ nanopore size control, which would be a vital tool  
6  
7 in generating effective and broadly functioning nanopore devices.  
8  
9

10  
11 The preparation of GNFs were produced by breaking down single-wall carbon.<sup>49</sup> The aqueous  
12  
13 GNF dispersions were prepared by dispersing 1, 1.5, and 3 mg of GNFs in 1.00 g of distilled  
14  
15 water and gentle stirring. Quartz nanopipettes were engineered from micro-capillaries (inner  
16  
17 diameter 0.5mm and outer diameter 1mm). The pipettes were fabricated with a laser based  
18  
19 puller.<sup>5,12,50</sup> The pulling diameter generated pipettes with an average nanopore sizes of 25 nm ( $\pm 2$   
20  
21 nm) across 20 pipettes, which was estimated from pore conductance measurements (full details  
22  
23 are available in the supplementary information). These pipettes were then dipped into the GNF  
24  
25 dispersions and withdrawn at a rate of 10 mm s<sup>-1</sup>. The pipettes were air dried for 10 min with the  
26  
27 pipette tips pointing vertically downwards. The pipettes were then placed in ceramic boats and  
28  
29 placed inside a quartz tube attached to a high vacuum system and heated to 900°C over a period  
30  
31 of 90 minutes (Figure 1A). Once cooled, the nanopipettes were sealed in air-tight containers and  
32  
33 only removed to be analysed.  
34  
35  
36  
37  
38  
39  
40  
41  
42  
43  
44  
45  
46  
47  
48  
49  
50  
51  
52  
53  
54  
55  
56  
57  
58  
59  
60

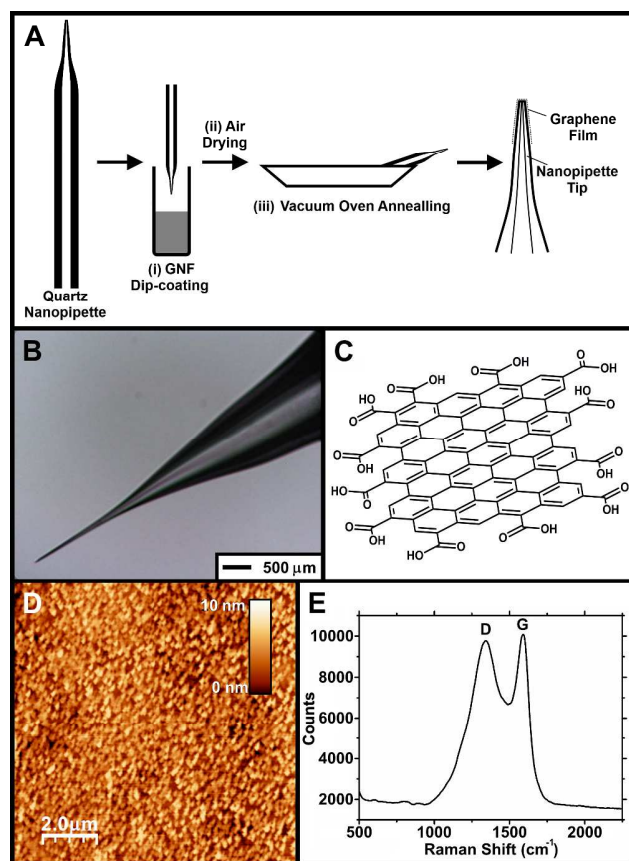


**Figure 1.** (A) Nanopipette coating schematic. Steps include; (i) dip-coating into GNF solutions of various concentrations, (ii) pipettes were left pointing with tips pointing downwards for 10 minutes of air drying and (iii) vacuum annealing was carried out at 900°C and a pressure of  $\sim 1.5 \times 10^{-5}$  mbar. (B) Shows an optical image of the nanopipette (scale bar inset). (C) A cartoon of an individual small GNF. The size of each GNF is  $\sim 30$  nm, and the edges of the GNF are functionalised with carboxylic acid groups (D) AFM image of a spin-coated GNFs annealed on a quartz substrate. The spin coating was carried out using a  $1.5 \text{ mg mL}^{-1}$  GNF solution, at a spin speed of 5000 rpm for 30 seconds. The individual features ( $\phi$  - *ca.* 30 nm) are the annealed GNFs, the measured surface roughness indicates a multi-layered arrangement (scale bar inset). (E) Raman spectra of the annealed GNF film on a quartz substrates. The characteristic D and G bands present in graphene are indicated on the spectrum.

The characterisation of GNF deposition has been previously reported which showed single sheet flakes of approx. 30 nm distributed homogenously along substrate surfaces.<sup>49</sup> An illustration of an individual GNF is shown in figure 1C. Deposition and the annealing of GNFs on quartz substrates were carried out to validate the resulting graphene materials. Uniform coatings of GNFs were achieved by spin-coating aqueous suspensions of various concentrations,

1  
2  
3 which were subsequently annealed (Figure 1). The surface roughness of the deposited films was  
4 analysed using AFM (Figure 1D). This showed the annealed GNFs ( $\phi \sim 30$  nm), and surface  
5 features that were no taller than 10 nm. The surface roughness of the underlying substrate was  
6 also analysed using AFM (Supplementary information – Figure S-1). The maximum surface  
7 feature was measured as 5 nm, the additional surface roughness (+ 5 nm) caused by the graphene  
8 coating suggests a film consisting of multiple graphene layers. The resultant graphitic material  
9 was also analysed using Raman spectroscopy (Figure 1E), which showed the D and G-bands  
10 expected for a graphene film. The presence of an intense D-band indicates a film containing  
11 defects, i.e. not perfectly graphenic carbon. This imperfection is brought about by the  
12 ‘patchwork’ nature of the resulting film, composed of annealed GNFs. XPS analysis was carried  
13 out on the coatings (Supplementary information – Figure S-2). In summary, the films were  
14 confirmed to be made up of defect-containing graphene, stacked into multiple layers (estimated  
15 at  $\sim 5$  nm).  
16  
17  
18  
19  
20  
21  
22  
23  
24  
25  
26  
27  
28  
29  
30  
31  
32  
33  
34

35 The deposition of GNFs onto nanopipettes could not be achieved through a simple  
36 modification of a previously used GNF deposition technique (spin-coating or drop-casting). Dip-  
37 coating of the pipette tips (Figure 1) offered an adaptable coating method, which could be readily  
38 achieved. The spin coating experiments, carried out on flat substrates, were used to estimate the  
39 concentration required for a conformal coating. Various concentrations of GNF solutions were  
40 used in order to explore a variety of coating conditions. Subsequent to dip-coating, the pipettes  
41 were left to air dry for 10 minutes, with their tips pointing downward, which demonstrated the  
42 most consistent nanopore coverage. Further orientations for pipettes drying were carried out  
43 (including; pointing vertically upward and horizontally). However, this did not provide  
44 consistent nanopore coverage on the electrical measurement i.e. the I-V curve. When examined  
45  
46  
47  
48  
49  
50  
51  
52  
53  
54  
55  
56  
57  
58  
59  
60



1  
2  
3  
4 optically, there was no observed presence of coatings on the pipettes when using GNF solutions  
5  
6 of  $1.5 \text{ mg mL}^{-1}$  or less, however there was a slight darkening of pipettes coated using  $3 \text{ mg mL}^{-1}$ .  
7  
8 The annealed nanopipettes showed no change in overall appearance and shape (i.e. taper length,  
9  
10 colour and angle of tip). The coatings on the pipettes were imaged using both SEM and TEM  
11  
12 (Figure 2). SEM images of nanopipettes before and after the coating process show successful  
13  
14 closing of the nanopore. TEM images of the pipette shaft show film thicknesses ( $\sim 3\text{-}4 \text{ nm}$ ) for  
15  
16 the deposited material. A full experimental description is given in the supplementary  
17  
18 information.  
19  
20  
21  
22  
23  
24  
25  
26  
27  
28  
29  
30  
31  
32  
33  
34  
35  
36  
37  
38  
39  
40  
41  
42  
43  
44  
45  
46  
47  
48  
49  
50  
51  
52  
53  
54  
55  
56  
57  
58  
59  
60

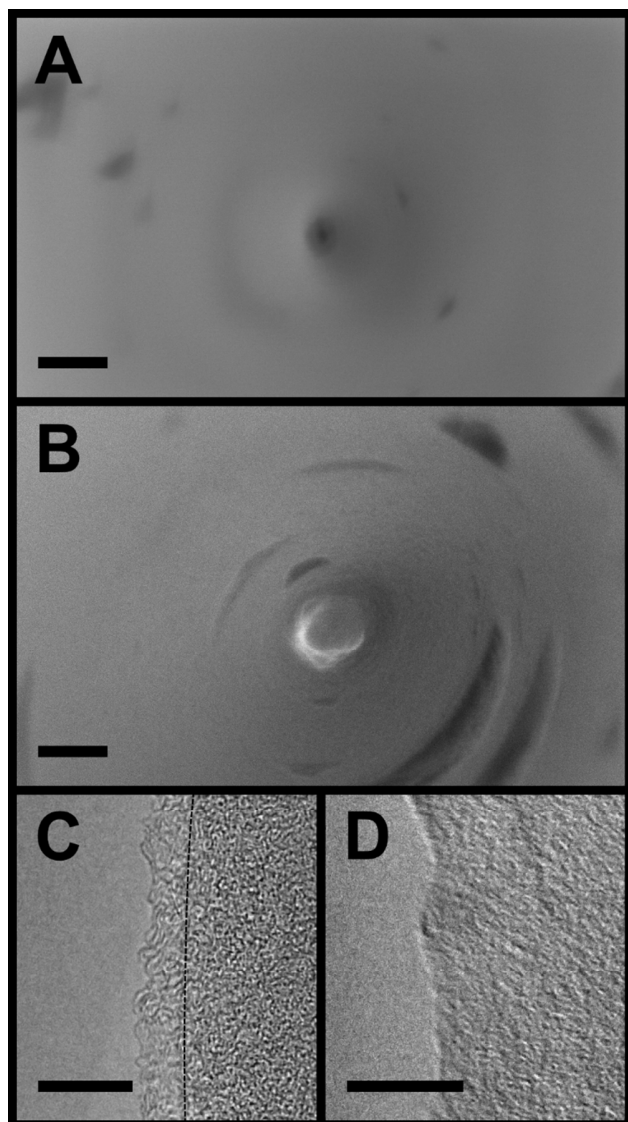


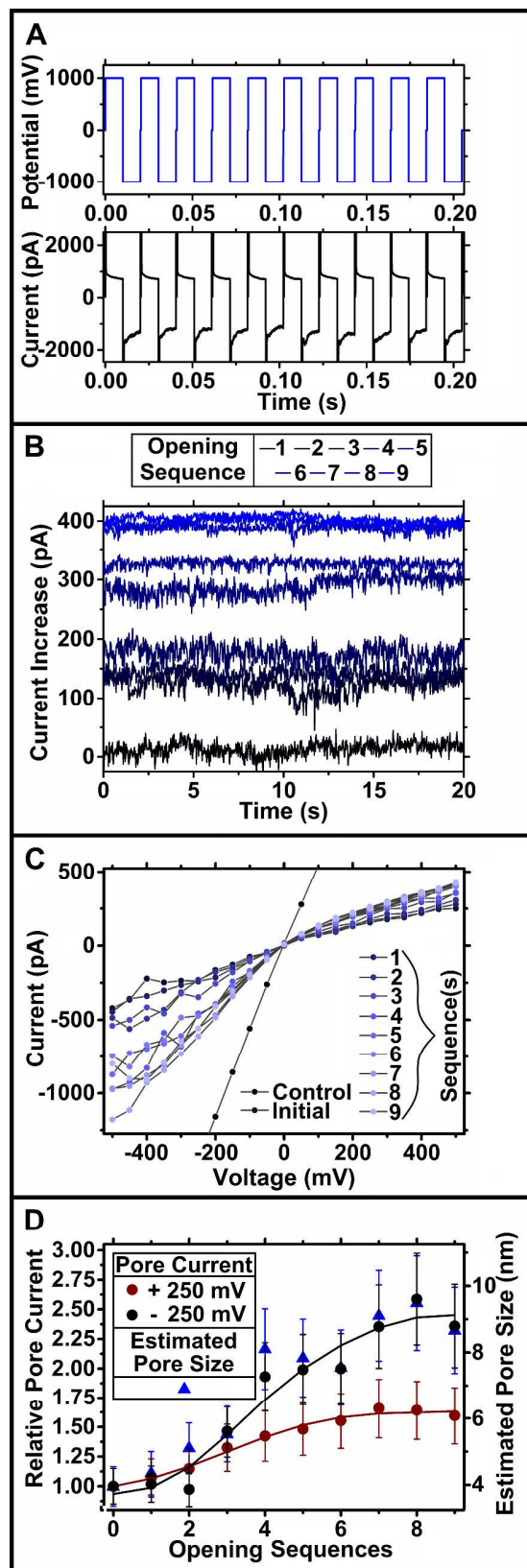
**Figure 2.** SEM images of (A) untreated and (B) GNF-coated nanopipettes. The untreated nanopipettes possess an average pore diameter of 25 nm. Scale bars of A/B show 100 nm. (C/D) TEM images of (C) GNF coated and (D) untreated nanopipettes edges. The GNF-coated pipettes have a 3-4 nm coating of material on the surface. The dashed line on image C indicates the line of the underlying quartz of the pipette. Scale bars of C/D show 10 nm. The coated pipettes in the images are treated with  $1.5 \text{ mg mL}^{-1}$  of GNF solutions before being annealed.

The nanopore size was also estimated through conductivity measurements. The uncoated pipettes showed a conductance of  $4.3 \text{ nS} (\pm 0.3 \text{ nS})$  at  $0.1 \text{ M KCl}$ . This is estimated to a pore size of  $25 \text{ nm} (\pm 2 \text{ nm})$  according to the model described by Steinbock et al.<sup>51</sup> The estimated pore

1  
2  
3 diameters were also comparable to literature recently reported.<sup>5</sup> This value did not change upon  
4  
5  
6 undergoing the annealing process. Graphene deposition provided pore blockages for the majority  
7  
8 of the treated pipettes at all concentrations, with the relative amounts of blockages increasing  
9  
10 with concentration; 50% for 1 mg mL<sup>-1</sup>, 84 % for 1.5 mg mL<sup>-1</sup>, 93.5% for 3 mg mL<sup>-1</sup>. The  
11  
12 graphene-coated pipettes showed average conductance value ( $7 \pm 0.8$  pS) when electrically  
13  
14 tested, indicating that the nanopore is closed. The pore opening process was aimed at steadily  
15  
16 opening the membrane covering the nanopore. The protocol designed for opening uses a rapidly  
17  
18 alternating current ( $\pm 1.0$  V at a frequency of 100 Hz), the pore opening was monitored by  
19  
20 measuring current flow and subsequent *I-V* measurements (Figure 3). This opening technique  
21  
22 was selected as graphene materials has been shown to exhibit delamination and redox chemistry  
23  
24 under an applied potential, while rapid reversal of applied potentials ensures a steady opening  
25  
26 process.<sup>52,53</sup>  
27  
28  
29  
30  
31

32  
33 Each opening sequence was carried out over a 200 second period. Typical current vs. time  
34  
35 traces are provided in the supplementary information (Figure S-3). The opening of multi-layered  
36  
37 graphene films was consistent for each concentration of GNF solutions used for dip coating. The  
38  
39 higher concentration solutions however gave films that required a greater number of opening  
40  
41 sequences to increase the pore size. The pipettes coated with 1.5 mg mL<sup>-1</sup> were found to be  
42  
43 optimal for opening experiments, providing a large amount of blocked pores, while also  
44  
45 providing steady opening for detecting DNA molecules. The average ratio of pore opening (final  
46  
47 pore diameter/untreated pore diameter) for these pipettes was  $\sim 0.7$ , which provided a large range  
48  
49 of pore sizes as the electroetching progressed. The lower proportion of blocked pipettes at lower  
50  
51 concentration is due to incomplete coverage achieved in the dip-coating process, with this  
52  
53 principle extended to more substantial GNF coating achieved at higher solution concentrations.  
54  
55  
56  
57  
58  
59  
60

1  
2  
3 The greater effort required to open the graphene films formed using higher GNF solution  
4 concentration was caused by the resultant carbonised coating being thicker and more consistent  
5 around the nanopipette. The pore opening process, could be primarily monitored through the  
6 current allowed to pass during the AC opening sequence (Figure 3A). The mean current flow  
7 would increase as the opening sequence was carried out (Figure 3B). This current flow is a direct  
8 indicator of the pore size, allowing for progressive monitoring as the opening sequence was  
9 applied. This was also used to gauge if a pore had reached its maximal size, with no increase  
10 observed throughout the sequence. After each opening sequence an  $I$ - $V$  measurements was taken  
11 to more accurately estimate the pore size (Figure 3C). Pipette coatings carried out using 1.5 mg  
12  $\text{mL}^{-1}$  could be opened with relative ease. Consecutive opening sequences resulted in the opening  
13 of the pore from fully closed to an estimated 9 nm in 9 sequences (Figure 3D). The thicker  
14 coatings generated by using 3 mg  $\text{mL}^{-1}$  were harder to open (Supplementary information –  
15 Figure S-4). The fully closed pores were commonly not open at all by numerous opening  
16 sequences. An optimal opening rate of 1.2 ( $\pm$  0.17) nm per sequence was achieved using an  
17 initial GNF solution of 1.5 mg  $\text{mL}^{-1}$ , this allowed for the size of the nanopore to be precisely  
18 tuned to detect specific analyte.  
19  
20  
21  
22  
23  
24  
25  
26  
27  
28  
29  
30  
31  
32  
33  
34  
35  
36  
37  
38  
39  
40  
41  
42  
43  
44  
45  
46  
47  
48  
49  
50  
51  
52  
53  
54  
55  
56  
57  
58  
59  
60

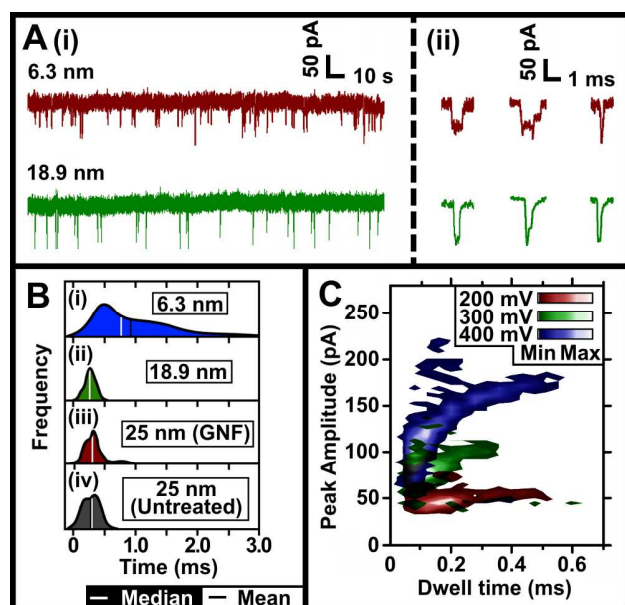


1  
2  
3 **Figure 3** - Pore opening data. (A) Shows a plot of the repeating square wave potential applied to  
4 the multi-layered graphene membranes. A corresponding current trace from a nanopore coated  
5 using  $1.5 \text{ mg mL}^{-1}$  of GNF solution is shown. (B) Shows the current increase/time trace for the  
6 first 20 seconds of each pore opening sequences for the same pipette, generated by using the  
7 average positive current flow (shown in 3A, from  $\sim 0$ -10 ms in the square wave cycle). The trend  
8 shows a general increase in current after each opening sequence. (C) Nanopipette  $I$ - $V$  plots after  
9 subsequent nanopore opening sequences. The pore opens from completely closed to a final  
10 estimate size of 8.7 nm after 9 sequences. (D) Shows a plot of the pore current at positive and  
11 negative potentials, as the pore is opened. The corresponding estimated pore size is also shown.  
12  
13  
14

15 The mechanism for the membrane opening could follow two main mechanisms, either *via*  
16 atom-by-atom removal or by sporadic flaking of the membrane, brought about by the  
17 electroetching of the graphene.<sup>52,53</sup> The opening rate of the multi-layered graphene membranes is  
18 somewhat consistent between opening sequences (Figure 3D). However, some fluctuation is seen  
19 in the current increase during the opening sequences (Figure 3B). Current flow was stable upon  
20 completion of the opening sequences, with similar baseline noise levels observed for both GNF-  
21 treated and un-treated nanopipettes (Supplementary information – Figure S-5). Opening  
22 occurring through an atom-by-atom removal would provide linear increases during the opening  
23 sequence. As this is not the case, a mechanism whereby masses of the graphene membrane is  
24 removed intermittently is most likely. However, pore opening data does not indicate the precise  
25 nature of this.  
26  
27  
28  
29  
30  
31  
32  
33  
34  
35  
36  
37  
38  
39  
40

41 The translocation behaviour of DNA was then studied, the aim was to monitor variations in  
42 translocation behaviour as the graphene membrane was opened. All of the reported DNA  
43 translocations were carried out using one type of DNA (10 kbp). With full characterisation of the  
44 translocation behaviour of the DNA carried out on untreated pipettes. Both the DNA  
45 concentration and ionic strength of the solution were kept constant throughout all reported  
46 experiments, however the potential applied to drive the translocations was varied. This change in  
47 applied potential provides differences in observed translocations (Figure 4). The current-time  
48  
49  
50  
51  
52  
53  
54  
55  
56  
57  
58  
59  
60

1  
2  
3  
4 traces show a positive spike in current as the DNA passes through, this is due to the extra charge  
5 carried by the DNA molecule. The features of each spike is characteristic of the pore properties,  
6 in addition to the conformation of the DNA as it passes through the nanopore (Figure 4A). The  
7 most important features of these traces are the dwell time (the total time for a translocation  
8 event), peak amplitude (the maximum height of a translocation peak from the baseline) and  
9 charge (the integrated area underneath the plotted translocation event). Detailed analysis of  
10 multiple translocation events reveals typical values of 0.37 ( $\pm 0.02$ ) ms, 59.3 ( $\pm 3.6$ ) pA and 17.1  
11 ( $\pm 2.17$ ) fA for dwell time, peak amplitude and charge respectively, at an applied potential of 300  
12 mV, using untreated nanopipettes.  
13  
14  
15  
16  
17  
18  
19  
20  
21  
22  
23  
24



25  
26  
27  
28  
29  
30  
31  
32  
33  
34  
35  
36  
37  
38  
39  
40  
41  
42  
43  
44  
45  
46  
47  
48 **Figure 4.** Translocation data for 10 kbp DNA through nanopores treated with multi-layered  
49 graphene membrane. (A) Current-time traces of DNA translocations through a GNF coated  
50 nanopores. Individual translocation events are also shown. (B) ‘Half-violin’ plots showing the  
51 average dwell time at different size of pore at various stages of opening, the overall trend shows  
52 the dwell time decreases as the pore diameter increases. (C) Translocation data from pipette  
53 membranes fabricated using an initial 1.5 mg mL<sup>-1</sup> GNF solution. The data shows the separation  
54 of DNA conformations as the applied potential is varied. All of the applied potentials have  
55 translocation events that occur at ~ 50 pA, this splits into two populations for both the 300 mV (~  
56 75 pA) and 400 mV (~125 pA) cases. The estimated pore size for this was ~ 22 nm.  
57  
58  
59  
60

1  
2  
3 The translocation of DNA was carried out in conjunction with the pore-opening experiments  
4 described above, with translocations attempted at each stage of opening process. The DNA  
5 solution used in each pipette was introduced using a MicroFil needle, the same DNA solution  
6 was used for all steps of opening and DNA sensing and was not exchanged at any point. The tip  
7 of the MicroFil needle was thin enough to reach the tip of the pipette, and so no air was trapped  
8 inside upon filling. The partially open pores, were then examined for differences in translocation  
9 behaviour. The current flow through the pore during translocations was found to be stable for the  
10 vast majority of nanopores at the various stages of opening. This made the observation of  
11 translocation events straightforward (Figure 4A). The systematic analysis of the coated pipettes  
12 found that there were no observed translocations using pipettes with pore sizes less than 6.3 nm,  
13 however there were bumping events at 5.52 nm, or alternatively this might due to the GNF flakes  
14 interacting with the DNA near the pore entrance. Additionally, fully opened nanopipettes  
15 showed moderate differences in translocation behaviour compared to measurements taken using  
16 non-coated pipettes (Figure 4B). This indicates that there was some interaction between the  
17 graphene coating and translocating DNA once the pipettes were fully opened. The major  
18 differences between these two cases include an increased average dwell time (from 0.37 ms to  
19 0.83 ms) at 300 mV, and increased the distribution of dwell times. These values compare well  
20 with reported nanopore devices fabricated from graphene membranes.<sup>54,55</sup> As the pore size was  
21 opened past 6.3 nm in size, translocations were observed. At these initially small nanopore sizes,  
22 the translocation events had longer dwell times (Figure 4B). This longer dwell time is caused by  
23 a range of factors, this includes the effect of confining the translocation volume, in addition to  
24 chemical interaction between the DNA and the graphene membrane. The reduction in pore size  
25 increases the energy barrier for DNA translocation. Another effect of the small pore sizes is that  
26  
27  
28  
29  
30  
31  
32  
33  
34  
35  
36  
37  
38  
39  
40  
41  
42  
43  
44  
45  
46  
47  
48  
49  
50  
51  
52  
53  
54  
55  
56  
57  
58  
59  
60



1  
2  
3  
4 the DNA must unravel in order to translocate, this conformation intrinsically has a longer  
5  
6 translocation time compared to a more constricted conformation. Additionally, the DNA may be  
7  
8 interacting significantly with the graphene coating as it passes through. The electrochemical  
9  
10 process used to open the pore may cause hydrophilic groups appearing at the surface, these  
11  
12 groups would act to attract the DNA molecules toward the membrane material – an effect that  
13  
14 would be greatest at smaller pore sizes.<sup>56</sup> The overall dwell time is reduced as the nanopore is  
15  
16 fully opened, which supports this concept.  
17  
18  
19

20  
21 DNA translocation detection depends heavily on the size of the nanopore used.<sup>28,29</sup> It was  
22  
23 found throughout the experiments that specific nanopore sizes lead to atypical observations of  
24  
25 DNA behaviour. This is exemplified by an example shown in figure 4C. The particular nanopore  
26  
27 was fabricated using an initial  $1.5 \text{ mg mL}^{-1}$  GNF, the pore was opened to an estimated diameter  
28  
29 of 22 nm. At an applied potential of 200 mV a single DNA population was observed indicating  
30  
31 an unfolded state of the molecules passes through the pore, however second populations  
32  
33 appeared when increased voltage at both 300 and 400 mV. Usually, we would expect this is due  
34  
35 to different conformations of the DNA passes the pore, however the excluded charge (integrated  
36  
37 current area per translocation event) values were very similar to 200 mV ( $5.43 \pm 2.2 \text{ fAs}$ ), only  
38  
39 increased by 1.5 fA as the voltage increased by 100 mV indicating other factors are affecting.  
40  
41 Another supporting information is that the uncoated nanopipette at 25 nm had an excluded  
42  
43 charge of  $13.95 \pm 3.01 \text{ fAs}$  at 200 mV which in agreement with other literature reported.<sup>12</sup> We  
44  
45 hypothesises this is due to the shape of the opening pore. Under typical circumstances the  
46  
47 nanopore would be thought to be circular, however the irregular multi-layer graphene coating  
48  
49 may have caused a non-circular opening in this case. As the size estimations are modelled on  
50  
51  
52  
53  
54  
55  
56  
57  
58  
59  
60

1  
2  
3 circular pores, this behaviour may be caused by a 'letter box' shaped pore, confining the  
4 translocation in one dimension, hence affecting the time of DNA passes through the pore.  
5  
6

7  
8  
9 The electrostatic interaction of the mobile ions with the nanopore surface charge is a factor that  
10 plays an important role in translocation behaviour in these devices to determine the device  
11 selectivity and rectification.<sup>57</sup> The untreated pipette has a rectification ratio of  $1.83 \pm 0.3$  at 0.1M  
12 KCl at pH 8.0 and this is consistent with other reported literatures.<sup>58,59</sup> The rectification ratio  
13 indicates the  $K^+$  ions flow more freely at negative applied potentials than positive potentials.  
14 The modified pipette at the same pH has a rectification ratio of  $2.67 \pm 0.52$  which is slightly  
15 higher than untreated nanopipette. This further enhances the selectivity and having a more  
16 negatively charged surface on the nanopipette. This may be caused by a number of factors,  
17 including; as the graphene coating is electro-etched and opened, there may be a functionality  
18 added to the surface such as negative carboxylate groups. This carboxylate groups could have  
19 respond to the electric field which then change the effective diameter of the pore and even  
20 closing it hence resulting higher rectification ratio.<sup>60</sup> Other characteristics that may contribute to  
21 surface charge effects include the electron density of the graphene coating.<sup>26</sup>  
22  
23  
24  
25  
26  
27  
28  
29  
30  
31  
32  
33  
34  
35  
36  
37  
38  
39

## 40 41 **Conclusion**

42  
43  
44 The present work demonstrates the *in-situ* controlled opening of nanopores *via* electroetching.  
45 The multi-layered graphene membranes are shown to be able to provide nanopores of any size  
46 between that of complete closure and fully opened pores. Through this we have achieve *in-situ*  
47 nanopore opening, allowing for the size to be varied as translocation experiments are carried out.  
48 The nanopipette devices demonstrate differences in DNA translocations, with small pores  
49 demonstrating very different in dwell time. These properties are facilitated by a targeted coating  
50  
51  
52  
53  
54  
55  
56  
57  
58  
59  
60

1  
2  
3 using GNFs (30 nm in diameter), to coat the nanopipette devices with a 25 nm diameter  
4 nanopore. The GNF films were annealed to form fully characterised graphene films. The film  
5 thickness was optimised to provide consistent coating and ease of opening. This was found to be  
6 obtained by using a 1.5 mg mL<sup>-1</sup> GNF solution for dip-coating, which provided a 3-4 nm thick  
7 film. Targeted nanopore opening will avoid the necessity to design and fabricate new nanopore  
8 architectures, as it is possible to tune the pore size to the analyte being probed. The technology  
9 reported also provides key benefits with respect to other reported techniques, such that the  
10 nanopipette fabrication and coating technique are both readily achieved and do not require any  
11 cleanroom fabrication. Use of graphene membranes is also compatible with surface  
12 functionalisation, and would provide a platform where surface chemistry could be tune to further  
13 explore a molecule of interest.  
14  
15  
16  
17  
18  
19  
20  
21  
22  
23  
24  
25  
26  
27  
28  
29

30 **Supporting Information.** The accompanying supporting information detail the following;  
31 experimental details, in addition to further materials and electrical characterisation. This material  
32 is available free of charge via the Internet at <http://pubs.acs.org>.  
33  
34  
35  
36  
37

#### 38 AUTHOR INFORMATION

#### 39 **Corresponding Author**

40  
41  
42 \*Joshua B. Edel – **Address** - Department of Chemistry, Imperial College London, South  
43 Kensington Campus, London, SW7 2AZ, United Kingdom. **Email** - [joshua.edel@imperial.ac.uk](mailto:joshua.edel@imperial.ac.uk)  
44  
45  
46  
47  
48

#### 49 **Author Contributions**

50  
51 The manuscript was written through contributions of all authors. All authors have given approval  
52 to the final version of the manuscript.  
53  
54  
55  
56  
57  
58  
59  
60

## ACKNOWLEDGMENTS

This work was supported in part by an ERC starting investigator grant (NanoP - 279818) and BBSRC grant (BB/L017865/1) to J.B.E. C.R.C. acknowledges support from the Ramsay Memorial Trust and C.G.S. the Royal Society (UF100144).

## REFERENCES

- (1) Fan, X.; White, I. M.; Shopova, S. I.; Zhu, H.; Suter, J. D.; Sun, Y. Sensitive Optical Biosensors for Unlabeled Targets: A Review. *Anal. Chim. Acta* **2008**, *620* (1–2), 8–26.
- (2) Ronkainen, N. J.; Halsall, H. B.; Heineman, W. R. Electrochemical Biosensors. *Chem. Soc. Rev.* **2010**, *39* (5), 1747–1763.
- (3) Turner, A. P. F. Biosensors: Sense and Sensibility. *Chem. Soc. Rev.* **2013**, *42* (8), 3184–3196.
- (4) Tamayo, J.; Kosaka, P. M.; Ruz, J. J.; Paulo, Á. S.; Calleja, M. Biosensors Based on Nanomechanical Systems. *Chem. Soc. Rev.* **2013**, *42* (3), 1287–1311.
- (5) Ivanov, A. P.; Actis, P.; Jönsson, P.; Klenerman, D.; Korchev, Y.; Edel, J. B. On-Demand Delivery of Single DNA Molecules Using Nanopipets. *ACS Nano* **2015**, *9* (4), 3587–3595.
- (6) Guo, X. Single-Molecule Electrical Biosensors Based on Single-Walled Carbon Nanotubes. *Adv. Mater.* **2013**, *25* (25), 3397–3408.
- (7) Okumoto, S.; Jones, A.; Frommer, W. B. Quantitative Imaging with Fluorescent Biosensors. *Annu. Rev. Plant Biol.* **2012**, *63* (1), 663–706.
- (8) Maragò, O. M.; Jones, P. H.; Gucciardi, P. G.; Volpe, G.; Ferrari, A. C. Optical Trapping and Manipulation of Nanostructures. *Nat. Nanotechnol.* **2013**, *8* (11), 807–819.
- (9) Lei, J.; Ju, H. Signal Amplification Using Functional Nanomaterials for Biosensing. *Chem. Soc. Rev.* **2012**, *41* (6), 2122–2134.
- (10) Branton, D.; Deamer, D. W.; Marziali, A.; Bayley, H.; Benner, S. A.; Butler, T.; Di Ventra, M.; Garaj, S.; Hibbs, A.; Huang, X.; Jovanovich, S. B.; Krstic, P. S.; Lindsay, S.; Ling, X. S.; Mastrangelo, C. H.; Meller, A.; Oliver, J. S.; Pershin, Y. V.; Ramsey, J. M.; Riehn, R.; Soni, G. V.; Tabard-Cossa, V.; Wanunu, M.; Wiggin, M.; Schloss, J. A. The Potential and Challenges of Nanopore Sequencing. *Nat. Biotechnol.* **2008**, *26* (10), 1146–1153.
- (11) Crick, C. R.; Albella, P.; Ng, B.; Ivanov, A. P.; Roschuk, T.; Cecchini, M. P.; Bresme, F.; Maier, S. A.; Edel, J. B. Precise Attoliter Temperature Control of Nanopore Sensors Using a Nanoplasmonic Bullseye. *Nano Lett.* **2015**, *15* (1), 553–559.

- 1  
2  
3  
4 (12) Gong, X.; Patil, A. V.; Ivanov, A. P.; Kong, Q.; Gibb, T.; Dogan, F.; deMello, A. J.;  
5 Edel, J. B. Label-Free In-Flow Detection of Single DNA Molecules Using Glass Nanopipettes.  
6 *Anal. Chem.* **2014**, *86* (1), 835–841.
- 7  
8 (13) Li, J.; Gershow, M.; Stein, D.; Brandin, E.; Golovchenko, J. A. DNA Molecules and  
9 Configurations in a Solid-State Nanopore Microscope. *Nat. Mater.* **2003**, *2* (9), 611–615.
- 10  
11 (14) Miles, B. N.; Ivanov, A. P.; Wilson, K. A.; Doğan, F.; Japrun, D.; Edel, J. B. Single  
12 Molecule Sensing with Solid-State Nanopores: Novel Materials, Methods, and Applications.  
13 *Chem. Soc. Rev.* **2012**, *42* (1), 15–28.
- 14  
15 (15) Ivanov, A. P.; Instuli, E.; McGilvery, C. M.; Baldwin, G.; McComb, D. W.; Albrecht, T.;  
16 Edel, J. B. DNA Tunneling Detector Embedded in a Nanopore. *Nano Lett.* **2011**, *11* (1), 279–  
17 285.
- 18  
19 (16) Pitchford, W. H.; Kim, H.-J.; Ivanov, A. P.; Kim, H.-M.; Yu, J.-S.; Leatherbarrow, R. J.;  
20 Albrecht, T.; Kim, K.-B.; Edel, J. B. Synchronized Optical and Electronic Detection of  
21 Biomolecules Using a Low Noise Nanopore Platform. *ACS Nano* **2015**, *9* (2), 1740–1748.
- 22  
23 (17) Cecchini, M. P.; Wiener, A.; Turek, V. A.; Chon, H.; Lee, S.; Ivanov, A. P.; McComb, D.  
24 W.; Choo, J.; Albrecht, T.; Maier, S. A.; Edel, J. B. Rapid Ultrasensitive Single Particle Surface-  
25 Enhanced Raman Spectroscopy Using Metallic Nanopores. *Nano Lett.* **2013**, *13* (10), 4602–  
26 4609.
- 27  
28 (18) Singer, A.; Rapireddy, S.; Ly, D. H.; Meller, A. Electronic Barcoding of a Viral Gene at  
29 the Single-Molecule Level. *Nano Lett.* **2012**, *12* (3), 1722–1728.
- 30  
31 (19) Brème, C.; Heslot, F. Mapping of Single-Base Differences between Two DNA Strands in  
32 a Single Molecule Using Holliday Junction Nanomechanics. *PLoS ONE* **2013**, *8* (2), e55154.
- 33  
34 (20) Han, C.; Hou, X.; Zhang, H.; Guo, W.; Li, H.; Jiang, L. Enantioselective Recognition in  
35 Biomimetic Single Artificial Nanochannels. *J. Am. Chem. Soc.* **2011**, *133* (20), 7644–7647.
- 36  
37 (21) Niedzwiecki, D. J.; Iyer, R.; Borer, P. N.; Movileanu, L. Sampling a Biomarker of the  
38 Human Immunodeficiency Virus across a Synthetic Nanopore. *ACS Nano* **2013**, *7* (4), 3341–  
39 3350.
- 40  
41 (22) Ali, M.; Neumann, R.; Ensinger, W. Sequence-Specific Recognition of DNA Oligomer  
42 Using Peptide Nucleic Acid (PNA)-Modified Synthetic Ion Channels: PNA/DNA Hybridization  
43 in Nanoconfined Environment. *ACS Nano* **2010**, *4* (12), 7267–7274.
- 44  
45 (23) Kowalczyk, S. W.; Hall, A. R.; Dekker, C. Detection of Local Protein Structures along  
46 DNA Using Solid-State Nanopores. *Nano Lett.* **2010**, *10* (1), 324–328.
- 47  
48 (24) Fanzio, P.; Mussi, V.; Menotta, M.; Firpo, G.; Repetto, L.; Guida, P.; Angeli, E.;  
49 Magnani, M.; Valbusa, U. Selective Protein Detection with a dsLNA-Functionalized Nanopore.  
50 *Biosens. Bioelectron.* **2015**, *64*, 219–226.
- 51  
52 (25) Ali, M.; Schiedt, B.; Neumann, R.; Ensinger, W. Biosensing with Functionalized Single  
53 Asymmetric Polymer Nanochannels. *Macromol. Biosci.* **2010**, *10* (1), 28–32.
- 54  
55  
56  
57  
58  
59  
60

- 1  
2  
3  
4 (26) Liu, K.; Feng, J.; Kis, A.; Radenovic, A. Atomically Thin Molybdenum Disulfide  
5 Nanopores with High Sensitivity for DNA Translocation. *ACS Nano* **2014**, *8* (3), 2504–2511.  
6  
7 (27) Luan, B.; Stolovitzky, G.; Martyna, G. Slowing and Controlling the Translocation of  
8 DNA in a Solid-State Nanopore. *Nanoscale* **2012**, *4* (4), 1068–1077.  
9  
10 (28) Sauer-Budge, A. F.; Nyamwanda, J. A.; Lubensky, D. K.; Branton, D. Unzipping  
11 Kinetics of Double-Stranded DNA in a Nanopore. *Phys. Rev. Lett.* **2003**, *90* (23), 238101.  
12  
13 (29) Mara, A.; Siwy, Z.; Trautmann, C.; Wan, J.; Kamme, F. An Asymmetric Polymer  
14 Nanopore for Single Molecule Detection. *Nano Lett.* **2004**, *4* (3), 497–501.  
15  
16 (30) Choi, S. S.; Park, M.-J.; Yamaguchi, T.; Kim, S.-I.; Park, K.-J.; Park, N. K. Fabrication  
17 of Nanopore on Pyramid. *Appl. Surf. Sci.* **2014**, *310*, 196–203.  
18  
19 (31) Li, N.; Yu, S.; Harrell, C. C.; Martin, C. R. Conical Nanopore Membranes. Preparation  
20 and Transport Properties. *Anal. Chem.* **2004**, *76* (7), 2025–2030.  
21  
22 (32) Chen, Z.; Jiang, Y.; Dunphy, D. R.; Adams, D. P.; Hodges, C.; Liu, N.; Zhang, N.;  
23 Xomeritakis, G.; Jin, X.; Aluru, N. R.; Gaik, S. J.; Hillhouse, H. W.; Jeffrey Brinker, C. DNA  
24 Translocation through an Array of Kinked Nanopores. *Nat. Mater.* **2010**, *9* (8), 667–675.  
25  
26 (33) Meng, H.; Xue, M.; Xia, T.; Zhao, Y.-L.; Tamanoi, F.; Stoddart, J. F.; Zink, J. I.; Nel, A.  
27 E. Autonomous in Vitro Anticancer Drug Release from Mesoporous Silica Nanoparticles by pH-  
28 Sensitive Nanovalves. *J. Am. Chem. Soc.* **2010**, *132* (36), 12690–12697.  
29  
30 (34) Freedman, K. J.; Ahn, C. W.; Kim, M. J. Detection of Long and Short DNA Using  
31 Nanopores with Graphitic Polyhedral Edges. *ACS Nano* **2013**, *7* (6), 5008–5016.  
32  
33 (35) Garaj, S.; Liu, S.; Golovchenko, J. A.; Branton, D. Molecule-Hugging Graphene  
34 Nanopores. *Proc. Natl. Acad. Sci. U. S. A.* **2013**, *110* (30), 12192–12196.  
35  
36 (36) Wells, D. B.; Belkin, M.; Comer, J.; Aksimentiev, A. Assessing Graphene Nanopores for  
37 Sequencing DNA. *Nano Lett.* **2012**, *12* (8), 4117–4123.  
38  
39 (37) Schneider, G. F.; Xu, Q.; Hage, S.; Luik, S.; Spoor, J. N. H.; Malladi, S.; Zandbergen, H.;  
40 Dekker, C. Tailoring the Hydrophobicity of Graphene for Its Use as Nanopores for DNA  
41 Translocation. *Nat. Commun.* **2013**, *4*.  
42  
43 (38) Nam, S.; Choi, I.; Fu, C.; Kim, K.; Hong, S.; Choi, Y.; Zettl, A.; Lee, L. P. Graphene  
44 Nanopore with a Self-Integrated Optical Antenna. *Nano Lett.* **2014**, *14* (10), 5584–5589.  
45  
46 (39) Shan, Y. P.; Tiwari, P. B.; Krishnakumar, P.; Vlassiouk, I.; Li, W. Z.; Wang, X. W.;  
47 Darici, Y.; Lindsay, S. M.; Wang, H. D.; Smirnov, S.; He, J. Surface Modification of Graphene  
48 Nanopores for Protein Translocation. *Nanotechnology* **2013**, *24* (49), 495102.  
49  
50 (40) Liu, S.; Zhao, Q.; Xu, J.; Yan, K.; Peng, H.; Yang, F.; You, L.; Yu, D. Fast and  
51 Controllable Fabrication of Suspended Graphene Nanopore Devices. *Nanotechnology* **2012**, *23*  
52 (8), 085301.  
53  
54  
55  
56  
57  
58  
59  
60

- 1  
2  
3  
4 (41) Shankla, M.; Aksimentiev, A. Conformational Transitions and Stop-and-Go Nanopore  
5 Transport of Single-Stranded DNA on Charged Graphene. *Nat. Commun.* **2014**, *5*.
- 6  
7 (42) Qiu, W.; Skafidas, E. Detection of Protein Conformational Changes with Multilayer  
8 Graphene Nanopore Sensors. *ACS Appl. Mater. Interfaces* **2014**, *6* (19), 16777–16781.
- 9  
10 (43) Walker, M. I.; Weatherup, R. S.; Bell, N. A. W.; Hofmann, S.; Keyser, U. F. Free-  
11 Standing Graphene Membranes on Glass Nanopores for Ionic Current Measurements. *Appl.*  
12 *Phys. Lett.* **2015**, *106* (2), 023119.
- 13  
14 (44) Feng, J.; Liu, K.; Graf, M.; Lihter, M.; Bulushev, R. D.; Dumcenco, D.; Alexander, D. T.  
15 L.; Krasnozhan, D.; Vuletic, T.; Kis, A.; Radenovic, A. Electrochemical Reaction in Single  
16 Layer MoS<sub>2</sub>: Nanopores Opened Atom by Atom. *Nano Lett.* **2015**, *15* (5), 3431–3438.
- 17  
18 (45) Briggs, K.; Charron, M.; Kwok, H.; Le, T.; Chahal, S.; Bustamante, J.; Waugh, M.;  
19 Tabard-Cossa, V. Kinetics of Nanopore Fabrication during Controlled Breakdown of Dielectric  
20 Membranes in Solution. *Nanotechnology* **2015**, *26* (8), 084004.
- 21  
22 (46) Kwok, H.; Briggs, K.; Tabard-Cossa, V. Nanopore Fabrication by Controlled Dielectric  
23 Breakdown. *PLoS ONE* **2014**, *9* (3), e92880.
- 24  
25 (47) Banerjee, S.; Shim, J.; Rivera, J.; Jin, X.; Estrada, D.; Solovyeva, V.; You, X.; Pak, J.;  
26 Pop, E.; Aluru, N.; Bashir, R. Electrochemistry at the Edge of a Single Graphene Layer in a  
27 Nanopore. *ACS Nano* **2013**, *7* (1), 834–843.
- 28  
29 (48) Kuan, A. T.; Lu, B.; Xie, P.; Szalay, T.; Golovchenko, J. A. Electrical Pulse Fabrication  
30 of Graphene Nanopores in Electrolyte Solution. *Appl. Phys. Lett.* **2015**, *106* (20), 203109.
- 31  
32 (49) Salzman, C. G.; Nicolosi, V.; Green, M. L. H. Edge-Carboxylated Graphene Nanoflakes  
33 from Nitric Acid Oxidised Arc-Discharge Material. *J. Mater. Chem.* **2009**, *20* (2), 314–319.
- 34  
35 (50) Sze, J. Y. Y.; Kumar, S.; Ivanov, A. P.; Oh, S.-H.; Edel, J. B. Fine Tuning of  
36 Nanopipettes Using Atomic Layer Deposition for Single Molecule Sensing. *Analyst* **2015**, *140*  
37 (14), 4828–4834.
- 38  
39 (51) Steinbock, L. J.; Lucas, A.; Otto, O.; Keyser, U. F. Voltage-Driven Transport of Ions and  
40 DNA through Nanocapillaries. *Electrophoresis* **2012**, *33* (23), 3480–3487.
- 41  
42 (52) Ambrosi, A.; Chua, C. K.; Bonanni, A.; Pumera, M. Electrochemistry of Graphene and  
43 Related Materials. *Chem. Rev.* **2014**, *114* (14), 7150–7188.
- 44  
45 (53) Yang, X.; Peng, H.; Xie, Q.; Zhou, Y.; Liu, Z. Clean and Efficient Transfer of CVD-  
46 Grown Graphene by Electrochemical Etching of Metal Substrate. *J. Electroanal. Chem.* **2013**,  
47 *688*, 243–248.
- 48  
49 (54) Merchant, C. A.; Healy, K.; Wanunu, M.; Ray, V.; Peterman, N.; Bartel, J.; Fischbein, M.  
50 D.; Venta, K.; Luo, Z.; Johnson, A. T. C.; Drndić, M. DNA Translocation through Graphene  
51 Nanopores. *Nano Lett.* **2010**, *10* (8), 2915–2921.
- 52  
53  
54  
55  
56  
57  
58  
59  
60

- 1  
2  
3  
4 (55) Banerjee, S.; Wilson, J.; Shim, J.; Shankla, M.; Corbin, E. A.; Aksimentiev, A.; Bashir,  
5 R. Slowing DNA Transport Using Graphene–DNA Interactions. *Adv. Funct. Mater.* **2015**, *25* (6),  
6 936–946.  
7  
8 (56) Yuan, W.; Zhou, Y.; Li, Y.; Li, C.; Peng, H.; Zhang, J.; Liu, Z.; Dai, L.; Shi, G. The  
9 Edge- and Basal-Plane-Specific Electrochemistry of a Single-Layer Graphene Sheet. *Sci. Rep.*  
10 **2013**, *3*.  
11  
12 (57) Umehara, S.; Pourmand, N.; Webb, C. D.; Davis, R. W.; Yasuda, K.; Karhanek, M.  
13 Current Rectification with Poly-L-Lysine-Coated Quartz Nanopipettes. *Nano Lett.* **2006**, *6* (11),  
14 2486–2492.  
15  
16 (58) Wei, C.; Bard, A. J.; Feldberg, S. W. Current Rectification at Quartz Nanopipet  
17 Electrodes. *Anal. Chem.* **1997**, *69* (22), 4627–4633.  
18  
19 (59) Sa, N.; Baker, L. A. Experiment and Simulation of Ion Transport through Nanopipettes of  
20 Well-Defined Conical Geometry. *J. Electrochem. Soc.* **2013**, *160* (6), H376–H381.  
21  
22 (60) Siwy, Z.; Gu, Y.; Spohr, H. A.; Baur, D.; Wolf-Reber, A.; Spohr, R.; Apel, P.; Korchev,  
23 Y. E. Rectification and Voltage Gating of Ion Currents in a Nanofabricated Pore. *Europhys. Lett.*  
24 **2002**, *60* (3), 349.  
25  
26  
27  
28  
29  
30  
31  
32  
33  
34  
35  
36  
37  
38  
39  
40  
41  
42  
43  
44  
45  
46  
47  
48  
49  
50  
51  
52  
53  
54  
55  
56  
57  
58  
59  
60



## Table of Contents Graphic

